Letter | Editors' Suggestion

Coupled instabilities drive quasiperiodic order-disorder transitions in Faraday waves

Valeri Frumkin [*,†]
Department of Mathematics, Massachusetts Institute of Technology, Cambridge, Massachusetts 02139, USA

Shreyas Gokhale [*,‡]
Department of Physics, Massachusetts Institute of Technology, Cambridge, Massachusetts 02139, USA

(Received 10 November 2022; revised 25 February 2023; accepted 31 May 2023; published 17 July 2023)

We present an experimental study of quasiperiodic transitions between a highly ordered square-lattice pattern and a disordered, defect-riddled state, in a circular Faraday system. We show that the transition is driven initially by a long-wave amplitude modulation instability, which excites the oscillatory transition phase instability, leading to the formation of dislocations in the Faraday lattice. The appearance of dislocations dampens amplitude modulations, which prevents further defects from being created and allows the system to relax back to its ordered state. The process then repeats itself in a quasiperiodic manner. Our experiments reveal an unexpected mechanism for temporal quasiperiodicity that results from a coupling between two distinct instabilities on the route to chaos.

DOI: 10.1103/PhysRevE.108.L012601

When a thin layer of fluid is subjected to uniform vertical vibration with sufficiently large amplitude, the initially flat fluid surface destabilizes to an ordered pattern of subharmonic standing waves, known as Faraday waves [1]. The Faraday system has been the subject of numerous theoretical [2–4] and experimental [5–7] studies, and it serves as a canonical example of a nonlinear pattern-forming system [8,9]. Its importance, however, goes beyond the study of pattern formation, as it manifests in a wide range of physical systems across multiple length scales. Faraday waves have been observed in systems as disparate as Bose-Einstein condensates [10], soft elastic solids [11], and even bodies of vibrated living earthworms [12]. In pilot-wave hydrodynamics, locally excited Faraday waves store information about the trajectories of walking droplets [13–15], while in hydrodynamic superradiance they serve as the underlying mechanism for sinusoidal oscillations of the droplet emission rate [16].

Since the Faraday system is readily accessible in the laboratory, it allows for a detailed study of the complex transition from order to disorder in pattern-forming systems. Specifically, when the driving amplitude is increased well beyond the Faraday threshold, defects appear in the ordered Faraday lattice, leading to the emergence of spatial disorder through a process that came to be known as "defect-mediated turbulence" [17]. Defect formation typically occurs via secondary instabilities, such as transverse amplitude modulation instability [18–22], and the oscillatory transition phase instability [23]. In the former, the square Faraday pattern is modulated by long-wavelength oscillations normal to the air-fluid interface, leading to an eventual loss of long-range order with increasing driving amplitude. In the latter, spatially uncorrelated elastic waves are excited within the plane of the Faraday lattice, leading to the emergence of defects. In both cases, as the defects are formed, the square Faraday pattern exhibits a state of spatial intermittency where the ordered and disordered phases can coexist. With further increase in driving amplitude the pattern loses any long-range order and "melts" into a fully spatiotemporally disordered state [24,25].

A less known, but intriguing phenomenon is that of temporal intermittency in the order-disorder transition in the Faraday system. This phenomenon was first reported by Ezersky [26], who observed the resonant excitation of long-wavelength gravity waves whenever the group velocity of capillary waves was close to the gravity wave speed $C = \sqrt{gh}$, where h is the liquid depth, and g is the acceleration due to gravity. These gravity waves induced a transition to chaos via rapid generation of higher harmonics. The system then alternated quasiperiodically between an ordered state with low-frequency vibrations and a fully disordered state.

Here we describe a distinct form of quasiperiodic dynamics in the Faraday system. We first show that in the case of a circular bath, for specific values of the bath radius, the amplitude modulation instability occurs in the form of vibrational modes of a circular elastic membrane. The strength of the modulation increases continuously in time. Strikingly, these growing amplitude modulations resonantly amplify in-plane transverse polarized lattice vibrations associated with the oscillatory transition phase instability. The in-plane oscillations grow over time, eventually leading to a partial disordering of the lattice via generation of dislocations. The presence of defects dampens amplitude modulations, allowing the system to relax back to its ordered state by clearing out the dislocations. The process then repeats itself.

Our experimental system consisted of a circular bath, 190 mm in diameter, that contained a 5-mm-deep circular

*These authors contributed equally to this work.
†valerafr@mit.edu
‡gokhales@mit.edu

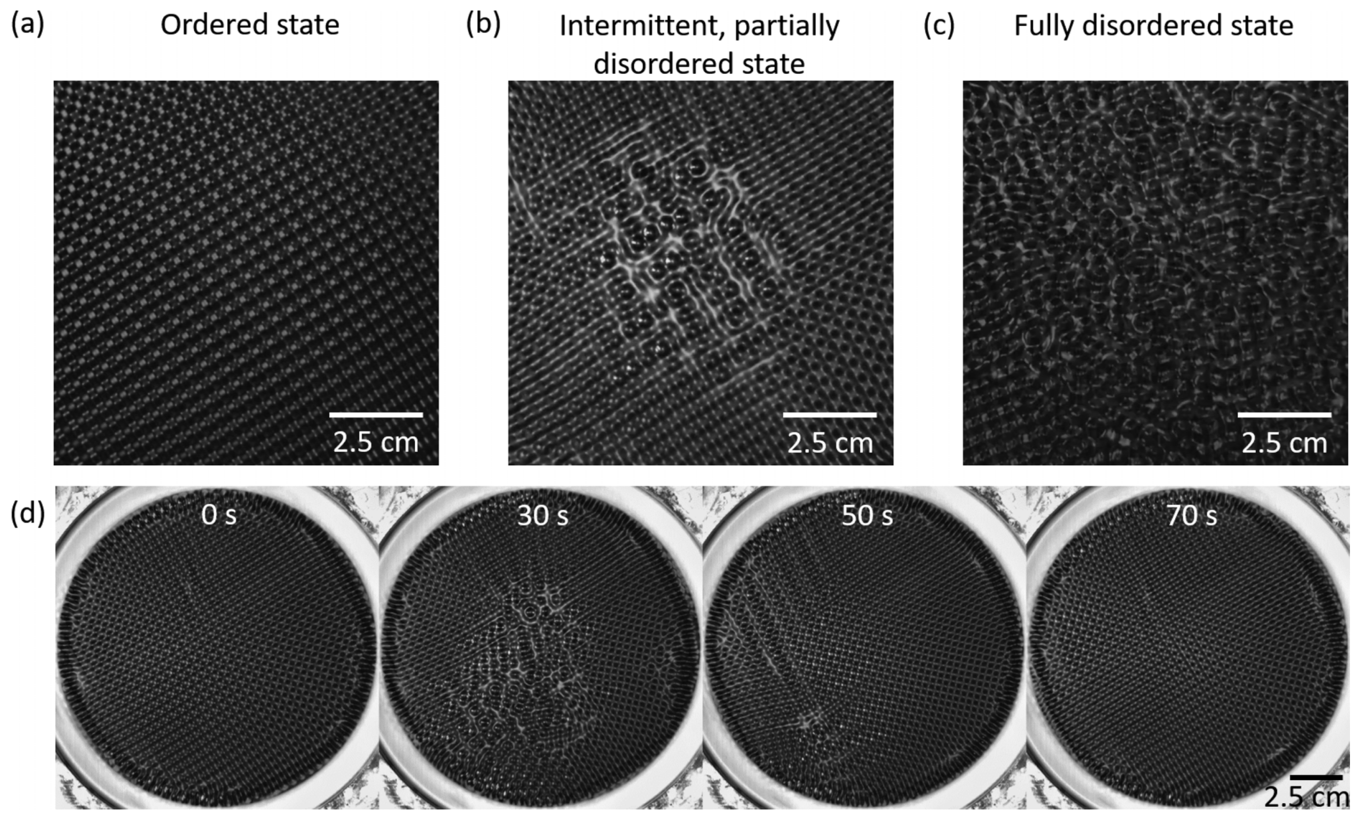

FIG. 1. Quasiperiodic transitions between order and disorder in Faraday waves. Snapshots of our system for a fixed driving frequency $f_d = 88$ Hz. (a) An ordered Faraday wave lattice at peak vibration acceleration $\gamma = 5.4g$, (b) an intermittent partially disordered state at $\gamma = 5.95g$, and (c) a fully disordered state at $\gamma = 6.5g$. (d) A time sequence of snapshots during a typical quasiperiod from the same data set as in (b), showing the onset of disorder followed by the clearing of defects and reordering of the lattice.

opening, with a diameter of 156 mm. The bath was filled with silicone oil so that the resulting oil depth was 5.6 ± 0.2 mm above the inner opening, and ≈ 0.6 mm in the surrounding shallow layer. The shallow layer acted as a wave damper and eliminated any effects due to sloshing of oil against the boundaries of the system. The silicone oil had surface tension $\sigma = 0.0209$ N/m, viscosity $\nu = 20$ cSt, and density $\rho = 0.965 \times 10^3$ kg/m^3. The bath was vibrated vertically by an electromagnetic shaker [27] with forcing $F(t) = \gamma \cos(2\pi f_d t)$, with f_d and γ being the frequency and peak vibrational acceleration, respectively. A detailed description of the experimental setup is given in the Supplemental Material (SM) [28].

Figure 1 describes the typical evolution of the Faraday system with increasing driving amplitude γ. For γ slightly above the pattern-forming threshold, the Faraday pattern takes the form of a square lattice characterized by highly coherent long-range order [Fig. 1(a)]. With further increase in the driving amplitude, line dislocations appear in the lattice leading to a regime of coexistence between ordered and disordered regions, reminiscent of the intermittency route to chaos [Fig. 1(b)]. The dislocation density increases with an increase in the driving amplitude, until finally the lattice "melts" into a fully disordered state [Fig. 1(c)].

The behavior of the system studied here is in stark contrast with the typical intermittency route to chaos. Specifically, there appears to be a small parameter range $\gamma_1 < \gamma < \gamma_2$, with γ_1 above the pattern-forming threshold and γ_2 below the dislocation-forming threshold, where amplitude modulations in the form of low-frequency gravity waves are excited. These secondary waves resonate with the driving frequency and grow in amplitude over time, leading to the formation of dislocations in the Faraday lattice. The presence of dislocations causes the system to lose its coherence and the long-wavelength gravity waves are damped. In the absence of gravity waves, the formed dislocations exit the system through its boundaries, restoring the original form of a highly ordered square lattice. At this point, full coherence is restored, which resets the system for the next order-disorder-order cycle [Fig. 1(d)]. Over long periods of time, our system switches quasiperiodically between highly coherent ordered states, and those that are partially disordered (see Supplemental Material Video S1).

Notably, the low-frequency waves observed here seem to represent vibrational modes of a circular membrane, which is consistent with previous observations that the ordered Faraday lattice can exhibit elasticlike behavior [29]. Figures 2(a) and 2(b) show a comparison between two clear, but distinct long-wavelength modes observed at $f_d = 88$ Hz and $f_d = 79$ Hz, respectively. A comparison to theoretically predicted circular membrane modes is made in Figs. 2(c) and 2(d), showing the (2,2) and the (1,2) modes, respectively. We observe a quantitative agreement between the shape and wavelength of the predicted and measured modes, further supporting this conclusion (see SM text for details) [28]. Modes that are excited at other frequencies in the proximity of $f_d = 88$ Hz and $f_d = 79$ Hz, exhibit some combination

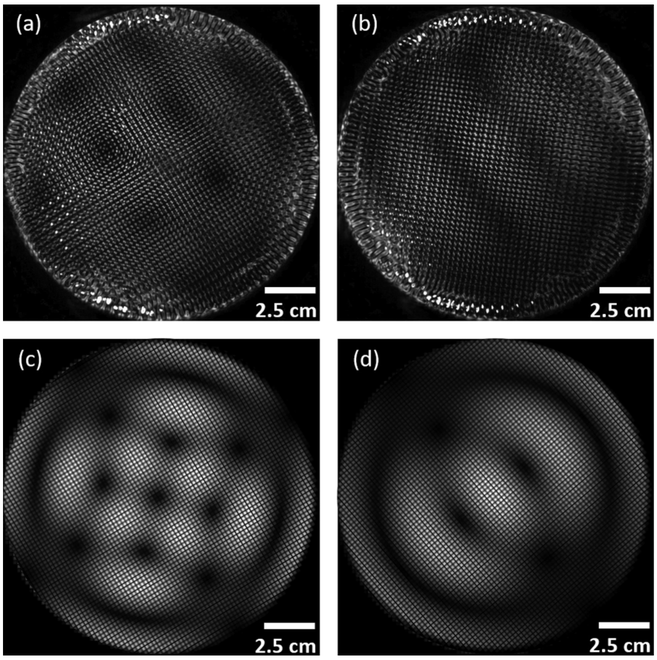

FIG. 2. Spatial structure of long-wavelength modes. (a), (b) Visualization of the spatial structure of long-wavelength modes for $f_d = 88$ Hz (a), and $f_d = 79$ Hz (b). The images in (a) and (b) represent the pixel-wise standard deviation of image intensity over one oscillation time period (≈ 1 s) leading up to disordering of the lattice. The image intensity has been uniformly multiplied by 3 to facilitate clearer visualization. (c), (d) Visualization of the geometry of theoretically predicted normal modes of a circular elastic membrane, with mode numbers (2,2) (c), and (1,2) (d). The membrane diameter in (c), and (d) is chosen to be the same as for experiments shown in (a) and (b).

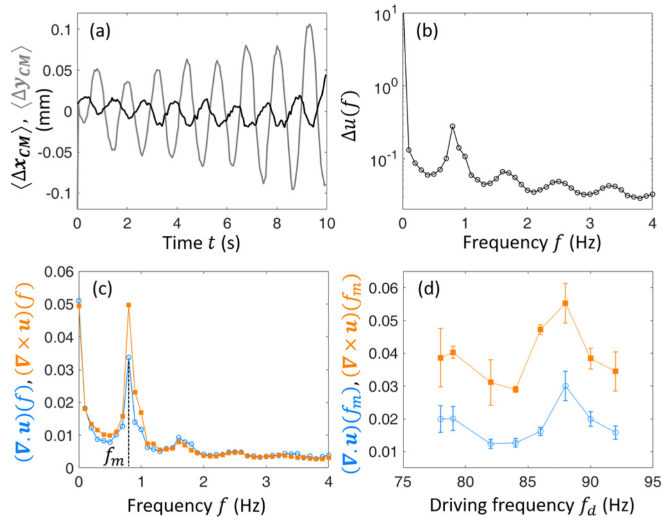

FIG. 3. Enhancement of transverse fluctuations due to resonant amplification of membrane modes. (a) Time series of the X (black) and Y (gray) coordinates of the center of mass prior to disordering of the lattice, for $f_d = 88$ Hz. (b) $\Delta u(f)$ versus frequency f for the same data as shown in (a), showing a prominent peak at the oscillation frequency of the long-wavelength mode. (c) Curl $\nabla \times \mathbf{u})(f)$ (filled orange squares) and divergence $(\nabla \cdot \mathbf{u})(f)$ (open blue circles) of displacements of intensity maxima as a function of frequency f. The frequency corresponding to the peak, f_m, corresponds to the frequency of long-wavelength oscillations shown in (b). (d) The peak values of curl [$(\nabla \times \mathbf{u})(f_m)$, filled orange squares] and divergence [$(\nabla \cdot \mathbf{u})(f_m)$, open blue circles] of displacements of intensity maxima as a function of driving frequency f_d. Error bars are standard errors of the mean across three distinct quasiperiods.

of the two main modes observed here (see Supplemental Material Video S2 for a visualization of the development of these low-frequency modes in our experiments). The correspondence between the driving frequency and the duration of the ordered vs disordered states, is discussed in Fig. S2 and associated Supplemental Material text [28].

To quantitatively characterize the oscillations leading up to disorder, we tracked the positions of intensity maxima over a period of 10 s prior to disordering of the lattice, using Blair and Dufresne's MATLAB implementation of the Crocker-Grier algorithm [30]. The low-frequency vibrations associated with $f_d = 88$ Hz are clearly visible in the displacement of the X and Y components of the center of mass, $\langle \Delta x_{\text{c.m.}} \rangle$ (black) and $\langle \Delta y_{\text{c.m.}} \rangle$ (gray) [Fig. 3(a)]. To characterize the associated lattice vibrations, following [23], we quantified the Fourier spectrum of relative displacements between nearest-neighbor intensity maxima. Specifically, we computed

$$\Delta u(f) = \sqrt{\langle \Delta x_{m,n}(f) \rangle_{m,n}^2 + \langle \Delta y_{m,n}(f) \rangle_{m,n}^2}, \tag{1}$$

where $\Delta x_{m,n}(f)$ and $\Delta y_{m,n}(f)$ are magnitudes of the Fourier transforms of X and Y components of relative displacements between nearest neighbors m and n, respectively, and $\langle \cdot \rangle_{m,n}$ denotes averaging over all pairs of nearest neighbors. $\Delta u(f)$ exhibits a sharp maximum at $f \approx 0.8$ Hz [Fig. 3(b)], consistent with the low-frequency vibration shown in Fig. 3(a). A similar maximum is observed near $f \sim 1$ Hz for all driving frequencies studied (Fig. S3) [28]. Crucially, the sharp maximum in $\Delta u(f)$ is quite distinct from the appearance of a broad shoulder observed by Fineberg and co-workers [23] in the oscillatory transition phase. To further compare and contrast our results with prior work, we computed the magnitude of the Fourier transform of the curl and divergence of displacements $\mathbf{u}(\mathbf{r}, t)$, $(\nabla \times \mathbf{u})(f)$ and $(\nabla \cdot \mathbf{u})(f)$, respectively, averaged over space. In the oscillatory transition phase [23], no enhancement is observed for $(\nabla \cdot \mathbf{u})(f)$, whereas a broad spectrum of frequencies are excited for $(\nabla \times \mathbf{u})(f)$. This corresponds to damped oscillatory waves with purely transverse polarization. In stark contrast, we observe that both $(\nabla \cdot \mathbf{u})(f)$ and $(\nabla \times \mathbf{u})(f)$ develop a sharp peak at a characteristic frequency [Fig. 3(c)]. Furthermore, we consistently observe that the peak in curl has a larger amplitude than the peak in divergence for all driving frequencies studied [Fig. 3(d)].

In practice, the signal in $(\nabla \cdot \mathbf{u})(f)$ derives from low-frequency modulations in the height of the fluid-air interface, which lead to apparent in-plane contractions and dilations in the positions of intensity maxima. However, the fact that these modulations lead to an enhancement in $(\nabla \times \mathbf{u})(f)$ suggests that low-frequency gravity wave modulations lead to resonant amplification of certain modes associated with the transverse oscillatory instability observed in [23]. Importantly, $(\nabla \cdot \mathbf{u})(f)$ as well as $\nabla \times \mathbf{u})(f)$ exhibit a pronounced maximum at $f = 88$ Hz, and a weaker one at $f = 79$ Hz.

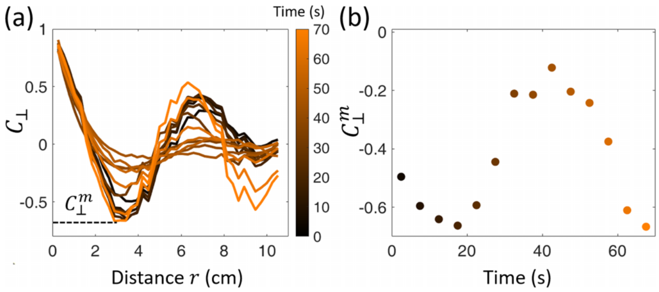

FIG. 4. Increase and decrease of coherence of long-wavelength modes within a quasiperiod. (a) The equal-time transverse-spatial velocity correlation $C_\perp$ averaged over time intervals of duration 5 s (100 frames) for the $f_d = 88$ Hz data shown in Fig. 1(d). The color changes with time from 0–5 s (black) to 65–70 s (light orange). The strongly negative correlations are consistent with the predominantly transverse polarization of long-wavelength oscillations. The more negative the minimum value $C_\perp^m$, the stronger are the correlations. (b) $C_\perp^m$ as a function of time during the quasiperiod. Colors correspond to the data in (a).

Consistent with these findings, we observed similar peaks in the timescale associated with the duration of the ordered state, as well as the characteristic timescale between two successive bursts of disorder (Fig. S2) [28].

In order to quantitatively characterize the sequence of increasing and decreasing coherence, we generated the velocity field for intensity maxima using the MATLAB package PIVLAB [31–33]. We then split our video into segments of duration 5 s (100 frames), and computed the equal-time transverse-spatial velocity correlation $C_\perp = \langle v_\perp(0) v_\perp(r)\rangle$ for each segment. Here, $v_\perp$ denotes the component of velocity perpendicular to the line joining two points on the particle image velocimetry (PIV) grid, and $\langle\cdot\rangle$ denotes averaging over the time interval of 5 s. Our choice of transverse velocity correlations was motivated by the fact that lattice vibrations have a predominantly transverse character [Figs. 3(c) and 3(d)]. Figure 4(a) shows the transverse velocity correlation for all 5-s time intervals within the 70-s duration shown in Fig. 1(d). At early (black) as well as late (light orange) times, when the lattice is ordered, we observe strong correlations that span almost the entire system. At intermediate times (brown), however, the strength of the correlations is reduced significantly due to disorder. To quantify the evolution of spatial coherence, we plotted the minimum value $C_\perp^m$ of the transverse spatial velocity correlations as a function of time [Fig. 4(b)]. $C_\perp^m$ initially becomes increasingly strongly negative, indicating increasingly strong correlations, as the membrane mode vibrations amplify transverse oscillations. Once the lattice disorders, $C_\perp^m$ quickly rises towards 0, as the oscillations lose coherence. At late times, the system becomes ordered again, and resonant amplification of the membrane mode once again results in $C_\perp^m$ reaching a strongly negative value.

Temporal quasiperiodicity is ubiquitous throughout various physical systems, and is often attributed to oscillations with time-dependent forcing, or to systems that oscillate with a finite number of incommensurable frequencies. Notable examples include El Ninó-Southern Oscillation in Climatology [34], quasiperiodic oscillation in x-ray astronomy [35], and quasiperiodic oscillations in dynamical systems [36]. Our findings reveal a mechanism for such quasiperiodic behavior based on an unexpected coupling between two instabilities associated with distinct routes to chaos, namely, transverse amplitude modulation and the oscillatory transition phase.

Our results differ from previous observations of temporal intermittency in the Faraday system in two significant ways. First, unlike the ripples observed by Ezersky [26], the initial amplitude modulation instability in our system takes the form of circular membrane modes. Secondly, instead of a cascade of higher harmonics leading to a fully disordered state, we observe the growth of in-plane lattice distortions that culminate in a *partially* disordered state. An interesting feature of our system is that the driving frequency (79 Hz $\leqslant f_d \leqslant$ 92 Hz) is orders of magnitude higher than the observed frequency of quasiperiods (~0.02 Hz). The characteristic timescales that give rise to quasiperiodicity in our system are therefore entirely emergent in nature, and derive solely from the positive and negative feedback between secondary instabilities. It is worth investigating whether, and to what extent, the mechanism for quasiperiodicity observed here applies to a broader class of driven-dissipative systems.

Finally, we note that our results bear intriguing connections to the observation of quasiperiodic strain bursts [37,38] associated with dislocation avalanches [39,40] in crystal plasticity. In crystal plasticity, the nonequilibrium drive is typically provided by an external mechanical deformation such as shear. Quasiperiodicity results from the interplay between dislocation motion and interactions as well as quenched disorder [37]. By contrast, in our system, lattice distortions are induced by secondary instabilities associated with the air-fluid interface. Further, spatial fluctuations in depth due to microscale surface roughness, as well as geometric frustration of the lattice near circular boundaries can serve as sources of quenched disorder in our system. Additionally, the generation of localized excitations such as oscillons, can also suppress wave propagation [41]. Thus, a detailed theoretical analysis of our results, possibly along the lines of studies on crystal plasticity, would be an exciting topic for future research.

All data are available in the main text, Supplemental Material, or from the authors upon request. All code is available from the authors upon request.

We thank John Bush for providing access to his laboratory, where these experiments were conducted. We also thank Denis Bartolo and Jay Fineberg for helpful comments on the manuscript. V.F. acknowledges the financial support of the National Science Foundation under Grant No. CMMI-2154151. S.G. acknowledges the Gordon and Betty Moore Foundation for support as a Physics of Living Systems Fellow through Grant No. GBMF4513.

The authors declare no competing interests.

[1] M. Faraday, XVII. On a peculiar class of acoustical figures; and on certain forms assumed by groups of particles upon vibrating elastic surfaces, Philos. Trans. R. Soc. London **121**, 299 (1831).

[2] T. B. Benjamin, F. J. Ursell, and G. I. Taylor, The stability of the plane free surface of a liquid in vertical periodic motion, Proc. R. Soc. London, Ser. A **225**, 505 (1954).
[3] J. Miles and D. Henderson, Parametrically forced surface waves, Annu. Rev. Fluid Mech. **22**, 143 (1990).
[4] J. Rajchenbach and D. Clamond, Faraday waves: Their dispersion relation, nature of bifurcation and wavenumber selection revisited, J. Fluid Mech. **777**, R2 (2015).
[5] W. S. Edwards and S. Fauve, Parametrically excited quasicrystalline surface waves, Phys. Rev. E **47**, R788(R) (1993).
[6] H. Arbell and J. Fineberg, Pattern formation in two-frequency forced parametric waves, Phys. Rev. E **65**, 036224 (2002).
[7] M.-T. Westra, D. J. Binks, and W. V. D. Water, Patterns of Faraday waves, J. Fluid Mech. **496**, 1 (2003).
[8] M. C. Cross and P. C. Hohenberg, Pattern formation outside of equilibrium, Rev. Mod. Phys. **65**, 851 (1993).
[9] J. P. Gollub and J. S. Langer, Pattern formation in nonequilibrium physics, Rev. Mod. Phys. **71**, S396 (1999).
[10] P. Engels, C. Atherton, and M. A. Hoefer, Observation of Faraday Waves in a Bose-Einstein Condensate, Phys. Rev. Lett. **98**, 095301 (2007).
[11] G. Bevilacqua, X. Shao, J. R. Saylor, J. B. Bostwick, and P. Ciarletta, Faraday waves in soft elastic solids, Proc. R. Soc. A **476**, 20200129 (2020).
[12] I. S. Maksymov and A. Pototsky, Excitation of Faraday-like body waves in vibrated living earthworms, Sci. Rep. **10**, 8564 (2020).
[13] A. Eddi, E. Sultan, J. Moukhtar, E. Fort, M. Rossi, and Y. Couder, Information stored in Faraday waves: The origin of a path memory, J. Fluid Mech. **674**, 433 (2011).
[14] J. W. Bush, Pilot-wave hydrodynamics, Annu. Rev. Fluid Mech. **47**, 269 (2015).
[15] J. W. M. Bush and A. U. Oza, Hydrodynamic quantum analogs, Rep. Prog. Phys. **84**, 017001 (2021).
[16] V. Frumkin, J. W. M. Bush, and K. Papatryfonos, Superradiant Droplet Emission from Parametrically Excited Cavities, Phys. Rev. Lett. **130**, 064002 (2023).
[17] P. Coullet, L. Gil, and J. Lega, A form of turbulence associated with defects, Phys. D (Amsterdam, Neth.) **37**, 91 (1989).
[18] A. Ezersii, M. Rabinovich, V. Reutov, and I. Starobinets, Spatiotemporal chaos in the parametric excitation of a capillary ripple, Zh. Eksp. Teor. Fiz. 91, 2070 (1986) [J. Exp. Theor. Phys. **64**, 1228 (1986)].
[19] N. B. Tufillaro, R. Ramshankar, and J. P. Gollub, Order-Disorder Transition in Capillary Ripples, Phys. Rev. Lett. **62**, 422 (1989).
[20] S. Douady, S. Fauve, and O. Thual, Oscillatory Phase Modulation of Parametrically Forced Surface Waves, Europhys. Lett. **10**, 309 (1989).
[21] S. T. Milner, Square patterns and secondary instabilities in driven capillary waves, J. Fluid Mech. **225**, 81 (1991).
[22] S. Ciliberto, S. Douady, and S. Fauve, Investigating space-time chaos in faraday instability by means of the fluctuations of the driving acceleration, Europhys. Lett. **15**, 23 (1991).
[23] I. Shani, G. Cohen, and J. Fineberg, Localized Instability on the Route to Disorder in Faraday Waves, Phys. Rev. Lett. **104**, 184507 (2010).
[24] E. Bosch and W. van de Water, Spatiotemporal Intermittency in the Faraday Experiment, Phys. Rev. Lett. **70**, 3420 (1993).
[25] D. I. Goldman, M. D. Shattuck, S. J. Moon, J. B. Swift, and H. L. Swinney, Lattice Dynamics and Melting of a Nonequilibrium Pattern, Phys. Rev. Lett. **90**, 104302 (2003).
[26] A. B. Ezersky, Temporal intermittency of chaos in parametrically excited capillary ripples, Europhys. Lett. **16**, 661 (1991).
[27] D. M. Harris and J. W. M. Bush, Generating uniaxial vibration with an electrodynamic shaker and external air bearing, J. Sound Vib. **334**, 255 (2015).
[28] See Supplemental Material at http://link.aps.org/supplemental/10.1103/PhysRevE.108.L012601 for details about experimental setup, quantification of timescales of quasiperiodic dynamics, and membrane mode analysis.
[29] L. Domino, M. Tarpin, S. Patinet, and A. Eddi, Faraday wave lattice as an elastic metamaterial, Phys. Rev. E **93**, 050202(R) (2016).
[30] J. C. Crocker and D. G. Grier, Methods of digital video microscopy for colloidal studies, J. Colloid Interface Sci. **179**, 298 (1996).
[31] W. Thielicke, The flapping flight of birds: Analysis and application, disseration thesis, University of Groningen, 2014.
[32] W. Thielicke and E. Stamhuis, PIVlab—Towards user-friendly, affordable and accurate digital particle image velocimetry in MATLAB, J. Open Res. Software **2**, e1 (2014).
[33] W. Thielicke and R. Sonntag, Particle image velocimetry for MATLAB: Accuracy and enhanced algorithms in PIVlab, J. Open Res. Software **9**, 1 (2021).
[34] C. Wang, A review of ENSO theories, Natl. Sci. Rev. **5**, 813 (2018).
[35] A. Ingram, M. van der Klis, M. Middleton, C. Done, D. Altamirano, L. Heil, P. Uttley, and M. Axelsson, A quasi-periodic modulation of the iron line centroid energy in the black hole binary H1743-322, Mon. Not. R. Astron. Soc. **461**, 1967 (2016).
[36] H. W. Broer, G. B. Huitema, and M. B. Sevryuk, *Quasi-Periodic Motions in Families of Dynamical Systems: Order amidst Chaos* (Springer, New York, 2009).
[37] S. Papanikolaou, D. M. Dimiduk, W. Choi, J. P. Sethna, M. D. Uchic, C. F. Woodward, and S. Zapperi, Quasi-periodic events in crystal plasticity and the self-organized avalanche oscillator, Nature (London) **490**, 517 (2012).
[38] Y. Cui, G. Po, and N. Ghoniem, Controlling Strain Bursts and Avalanches at the Nano- to Micrometer Scale, Phys. Rev. Lett. **117**, 155502 (2016).
[39] S. Papanikolaou, Y. Cui, and N. Ghoniem, Avalanches and plastic flow in crystal plasticity: An overview, Modell. Simul. Mater. Sci. Eng. **26**, 013001 (2018).
[40] F. F. Csikor, C. Motz, D. Weygand, M. Zaiser, and S. Zapperi, Dislocation avalanches, strain bursts, and the problem of plastic forming at the micrometer scale, Science **318**, 251 (2007).
[41] H. Arbell and J. Fineberg, Temporally Harmonic Oscillons in Newtonian Fluids, Phys. Rev. Lett. **85**, 756 (2000).